Kinetics of binding of fluorescent ligands to enzymes with engineered access tunnels

Shubhangi Kaushik[1], Zbynek Prokop[1, 2], Jiri Damborsky[1, 2], Radka Chaloupkova[1, 2#]

[1]Loschmidt Laboratories, Department of Experimental Biology and Research Centre for Toxic Compounds in the Environment RECETOX, Masaryk University, Brno, Czech Republic [2]International Clinical Research Center, St. Anne's University Hospital, Brno, Czech Republic

[#]Author for correspondence: radka@chemi.muni.cz

Article type : Original Articles

ABSTRACT

Molecular recognition mechanisms and kinetics of binding of ligands to buried active sites via access tunnels are not well understood. Fluorescence polarization enables rapid and non-destructive real-time quantification of the association between small fluorescent ligands and large biomolecules. In this study, we describe analysis of binding kinetics of fluorescent ligands resembling linear halogenated alkanes to haloalkane dehalogenases. Dehalogenases possess buried active sites connected to the surrounding solvent by access tunnels. Modification of these tunnels by mutagenesis has emerged as a novel strategy to tailor the enzyme properties. We demonstrate that the fluorescence polarization method can sense differences in binding kinetics originating from even single mutation introduced to the tunnels. The results show, strikingly, that the rate constant of the dehalogenase variants varied across seven orders of magnitude and the type of ligand used strongly affected the binding kinetics of the enzyme. Furthermore, fluorescence polarization could be applied to cell-free extracts instead of purified proteins, extending the method's application to medium-throughput screening of enzyme variant libraries generated in directed evolution experiments. The method can also provide in-depth kinetic information about the rate-determining step in binding kinetics and reveals the bottlenecks of enzyme accessibility. Assuming availability of appropriate fluorescent ligand, the method could be applied for analysis of accessibility of tunnels and buried active sites of enzymes forming a covalent alkyl-enzyme intermediate during their catalytic cycle, such as α/β-hydrolases containing >100,000 protein sequences based on the Pfam database.

Running title: Ligand binding to proteins with engineered tunnels

Keywords: Fluorescence polarization, binding kinetics, HaloTag ligands, haloalkane dehalogenases, modified access tunnels

List of abbreviation: FP; fluorescence polarization, NMR; nuclear magnetic resonance, CD; circular dichroism, MALDI-TOF MS; matrix-assisted laser desorption/ionization time-of-flight mass spectroscopy, TMR; tetramethylrhodamine, SDS-PAGE; sodium dodecyl sulfate polyacrylamide gel electrophoresis.

This article has been accepted for publication and undergone full peer review but has not been through the copyediting, typesetting, pagination and proofreading process, which may lead to differences between this version and the Version of Record. Please cite this article as doi: 10.1111/febs.13957

INTRODUCTION

Enzymes catalyze reactions with remarkable efficiency and specificity under mild conditions. Structurally, many enzymes have buried active sites connected with the surrounding solvent by several access pathways known as tunnels [1]. Tunnels have been identified across all classes of enzymes including hydrolases such as lipases [2-4], epoxide hydrolases [5, 6] and haloalkane dehalogenases [7-9]; ligases such as carbamoyl phosphate synthetases [10, 11]; transferases such as polynucleotide kinase [12]; oxidoreductases such as amine oxidase [13] and cytochrome P450s [14]; lyases such as hydroxynitrile lyase [15] and isomerases such as glutamate racemase [16]. Molecular tunnels have a regulatory role in enzymatic catalysis, mediating the access and egress of substrates, reactive intermediates, products, ions and solvent molecules [17]. The size, shape, dynamics and physicochemical properties of tunnels are important determinants of enzyme stability, catalytic activity, substrate specificity and enantioselectivity [18]. Access tunnels can be either permanent or transient features of enzymes, and have been investigated by X-ray crystallography, NMR spectroscopy, steady-state kinetics and molecular modeling [19, 20].

One of the primary objectives of protein engineering is the modification of enzyme properties for practical applications, generally either via random mutagenesis of the target gene, known as directed evolution, or via a rational strategy, in which detailed knowledge of protein structure, function and mechanism is applied to make specific alterations [21]. In recent years, tunnel residues have emerged as attractive targets for protein engineering as they represent natural hotspots for focused evolution. Mutagenesis of residues lining a tunnel does not disrupt the architecture of the active site, and thus increases the probability of construction of functional clones with evolved properties [21, 22]. This strategy has been successfully applied to many enzymes with buried active sites in attempts to improve their catalytic properties [20, 23-29]. For example, screening of a focused library in lipase led to identification of mutants displaying enhanced transacylation activity compared to hydrolytic activity due to blocked access tunnels [28]. Another study demonstrated the role of entropy in terpene cyclase catalyzed polycyclization reaction through point mutation in one of the water channels. The mutation caused disruption of a water channel leading to decreased contribution of entropy to catalysis and thus affected activity and selectivity of the enzyme [29].

Haloalkane dehalogenases (EC 3.8.1.5) are hydrolytic enzymes that cleave carbon-halogen bonds in halogenated hydrocarbons. They have important applications in bioremediation [30], biosensing [31], biosynthesis [32, 33], cellular imaging and protein analysis [34]. These enzymes possess an active site deeply buried in a hydrophobic cavity between two domains. The active site cavities of haloalkane dehalogenase DhaA from *Rhodococcus rhodochrous* NCIMB13064 [35] and LinB from *Sphingobium japonicum* UT26 [36], two enzymes analyzed in this study, are accessible to the solvent via the main and the slot tunnels. Previous efforts to modify access tunnels in DhaA generated variants with high stability in the presence of elevated temperature and organic co-solvents, but reduced catalytic activity in an aqueous environment [22, 37]. Further fine-tuning of the access tunnel geometry and dynamics led to a biocatalyst with better balance between activity and stability [38]. In another study, computationally identified hotspots in access tunnel of DhaA were targeted by focused mutagenesis and resulted in the mutant enzyme with substantially improved activity towards anthropogenic compound 1,2,3-trichloropropane [21]. The potential impact of tunnel modification on activity and specificity was also shown by site-directed mutagenesis of surface residue positioned at the tunnel entrance of haloalkane dehalogenase LinB [39].

Substitution of this bottleneck residue altered the tunnel size and thus modulated the enzyme activity and specificity [39].

A robust but convenient approach is required for quantitative analysis of biomolecular interactions and a candidate methodology is fluorescence polarization (FP), a solution-based technique that allows rapid real-time quantification of the association between a fluorescent ligand and a larger molecule [40, 41]. FP measures the intensity of light emitted parallel and perpendicular to the plane of excitation light. The association of small fluorescent molecule to a large biomolecule results in the changes in polarization in time until the equilibrium establishes [42]. The advantages of FP approach include its robust format, high sensitivity, non-destructive nature, homogeneity and that it is unaffected by absorptive interferences or inner filter effects. Moreover, the assay does not require the separation of bound and unbound ligand, which enables monitoring of the interaction between the small fluorescent ligand and the larger biomolecules without disturbing equilibrium [42, 43].

The study presented here focused on FP-based quantitative analysis of the binding kinetics of fluorescent HaloTag ligands to haloalkane dehalogenases with engineered access tunnels. There were five main goals. First, to determine whether the FP method is sufficiently sensitive to detect changes in the binding kinetics of fluorescent ligands to enzymes with different access tunnel mutations. Second, to study the effects of different HaloTag ligands on binding kinetics of studied enzymes. Third, to identify limits of FP methodology in determining binding behavior of enzymes with modified access tunnel geometries. Fourth, to use cell free extracts instead of purified enzymes in the assay to extend method applicability in medium-throughput screening of variant libraries from directed evolution experiments. Fifth, to explore whether rate-determining step in binding kinetics is enzyme-ligand association or chemical step involving S_N2 reaction leading to the formation of covalent complex.

RESULTS

Construction of H272F variants of haloalkane dehalogenases with modified access tunnels

A set of biochemically characterized variants of haloalkane dehalogenase DhaA and LinB exhibiting modifications in the access tunnel geometries were studied in the present work (Table 1). Application of the FP method to determine binding kinetics of fluorescent HaloTag ligands to the haloalkane dehalogenases with modified tunnels required covalent attachment between the ligands and selected enzymes. For this purpose, the catalytic base histidine was replaced by phenylalanine in all selected variants. During the catalytic cycle of the dehalogenation reaction, a covalent alkyl-enzyme intermediate is formed by nucleophilic attack of the carboxylate oxygen of an aspartate group on the carbon atom of the substrate. The alkyl-enzyme intermediate is subsequently hydrolyzed by a water molecule, which requires activation by a catalytic histidine [44]. Thus, variants with a phenylalanine substituted for the catalytic histidine cannot efficiently hydrolyze the alkyl-enzyme intermediate [45] and the reaction intermediate remains as a covalent complex (Fig. 1). The interaction between the chloroalkane linker moiety of the ligand and the dehalogenase structure is highly site-specific and irreversible in nature [34].

Site-directed mutagenesis was used to exchange the catalytic histidine with phenylalanine in selected DhaA and LinB haloalkane dehalogenase variants. The constructed histidine-substituted haloalkane dehalogenase variants with modified tunnels were overexpressed in *Escherichia coli* host cells and purified by metallo-affinity chromatography. All tested enzymes were prepared in a purity > 90% (Fig. 2A) according to SDS-PAGE analysis, which

is sufficient for further characterization of the enzymes by FP method. Far-UV CD spectroscopy was used to evaluate the effect of the H272F mutation on the folding and secondary structure of the enzyme variants. All of the enzymes tested exhibited CD spectra with one positive maximum at 195 nm and two negative maxima at 208 and 222 nm, characteristic of α-helical conformation [46]. This suggests that the incorporated substitution has no effect on overall secondary structure of the enzymes since no significant differences in shape and intensity of the spectra were observed between individual enzyme variants and the corresponding wild-type enzymes containing H272F mutation (Fig. 2B).

Binding kinetics of fluorescent ligands to DhaA and LinB variants with engineered tunnels

Two HaloTag ligands with distinct fluorophore moieties, Alexa Fluor 488 and TMR, were used to determine binding behavior of the DhaA and LinB haloalkane dehalogenases with modified access tunnels. During binding reactions the concentration of one of the reactants, usually the ligand was kept constant, while the concentration of the enzyme variant was in molar excess to drive the binding reaction to completion.

In binding experiments with Alexa Fluor 488, the reaction proceeded to completion within a few minutes with the commercially available HaloTag protein, DhaAHT+H272F (referred as DhaAHT* in the current work; for simplicity all variants containing H272F mutation will be marked with a star symbol), which has been optimized to form a covalent bond with HaloTag ligands [34, 47]. Several hours were required for completion of its binding to DhaAWT*, but less than an hour for its binding to the DhaA106* variant, which has similar access tunnel geometry to DhaAWT* (Fig. 3A). In contrast, no binding was observed with the variant DhaA31* carrying five bulky amino acid substitutions in the tunnel leading to the occluded active site cavity, which is a possible explanation why Alexa Fluor 488 cannot reach this variant's active site and form a covalent bond with the nucleophilic residue. All the tested LinB variants displayed slow binding rates usually completing the reaction in the time scale of several hours. LinB26* carrying the small residue at tunnel mouth, displayed improved binding rate compared to that of LinBWT* while LinB35* exhibited binding rate in similar range as that of LinBWT* (Fig. 3B). No binding of the ligand was observed in the case of LinB32* and LinB86*, most likely due to blocked access tunnel by introduced bulky Trp residue in tunnel mouth.

The TMR ligand binding to the DhaA and LinB variants was also tested (Figure 3, Table 2). The binding reaction of TMR with DhaAHT* finished within couple of minutes as reported previously [34, 47] while its binding to the variants DhaAWT* and DhaA106* took almost 2 and 1.5 hours, respectively (Fig. 3C). The binding rates determined for DhaAWT* are again in accordance with previous findings [34]. Interestingly, it was possible to determine the binding kinetics between TMR and DhaA31*, a variant that did not interact with Alexa Fluor 488 (Fig. 4, Table 2), confirming the influence of ligand structure on dehalogenase enzymes' binding kinetics and the importance of selecting appropriate ligands for assessing effects of modifications. The LinB variants LinB26* and LinB35* reacted with TMR significantly more rapidly than LinBWT* (Fig. 3D). The LinB32* and LinB86* variants did not interact with the TMR ligand. Generally, the LinB variants exhibited slower binding kinetics with both fluorescent ligands than the DhaA variants (Fig. 3, Table 2). The binding experiments with Alexa Fluor488 and TMR clearly demonstrates the importance of the fluorophore moiety structure for the binding kinetics of the tested haloalkane dehalogenases.

MALDI-TOF MS confirmed interactions between fluorescent ligands and enzyme variants

No changes in FP signals collected with LinB86* and LinB32* variants were detected following addition of TMR or Alexa Fluor 488, suggesting that these enzymes did not interact with either of the tested HaloTag fluorescent ligands. Both of these variants have a bulky Trp residue at the tunnel opening, which might prevent binding of the ligand at the enzyme active site. Tryptophan residue located at the tunnel entrance in close proximity to the fluorescent moiety may simultaneously cause quenching of the ligand fluorescence during the binding experiment, as described previously [48]. This would lead to an unmodified fluorescence polarization signal. Therefore, to determine whether the ligand can bind to the enzyme, samples of LinB32* and LinB86* in both free form and in solution with TMR ligand were subjected to MALDI-TOF MS analysis. The results show that neither LinB32* nor LinB86* formed a covalent complex with TMR, confirming that these enzyme variants do not interact with the TMR ligand and disproving the hypothesis that binding-associated fluorescence is quenched by the Trp residue (Fig. 5A and 5B). To further confirm the absence of interaction between these variants and ligands, the variants were digested by trypsin (in both free form and in solution with TMR) then analyzed by MALDI-MS/MS. No modification of the nucleophilic residue was observed, confirming that TMR had not reacted at the active site of either LinB variant (data not shown). MALDI-TOF MS spectra of LinBWT* and LinB26*, in free form and in conjunction with the TMR ligand, were used as positive controls, as these variants had clearly formed covalent complexes with both HaloTag ligands during FP experiments. The average masses of these variants increased when TMR was added and the change in mass corresponded well to the molecular mass of TMR (Fig. 5C and 5D). Hence, the TMR ligand was successfully incorporated into the structures of variants LinBWT* and LinB26*.

The FP experiments showed that DhaA31* did not interact with Alexa Fluor 488 but was able to form a covalent complex with the TMR ligand. To verify this selective binding interaction of DhaA31* with the TMR ligand, MALDI-TOF MS spectra of DhaA31* in free form and in solution with both ligands, were recorded. As expected, the average mass of DhaA31* did not change in the presence of Alexa Fluor 488, confirming that the enzyme and this ligand do not interact. In contrast, comparison of the molecular masses of DhaA31* in free form and in solution with TMR confirmed the successful incorporation of TMR into the enzyme structure (Fig. 6).

Effect of fluorophore moiety of the fluorescent ligands on binding kinetics

The FP experiments clearly showed that the ligands' fluorophore moiety affected the enzyme-ligand binding kinetics. We tested binding kinetics of another ligand, HaloTag R110 direct, to the haloalkane dehalogenase variants. The fluorophore moiety of this ligand differs from that of TMR by the presence of amide groups without methylated nitrogen atoms and from Alexa Fluor 488 by the absence of sulfonate groups. The binding of R110 direct ligand was much faster to LinB26* as compared to LinB35* variant (Table 3). Furthermore, R110 direct did not bind to LinB86*, similarly to Alexa Fluor 488 and TMR. Interestingly, there was no binding detected for R110 direct and DhaA31*. We conclude that TMR is the most suitable ligand for monitoring the binding kinetics of haloalkane dehalogenases with modified tunnels.

Applicability of fluorescence polarization assay for medium-throughput screening

To investigate the possibility of using cell free extract instead of purified enzymes in FP assay, the kinetics of TMR binding into cell free extracts of selected DhaA variants (DhaAWT*, DhaAHT*, DhaA31*) were analyzed and compared with the binding rates determined previously with purified enzymes. The reaction mixture was composed of the cell free extract, optimized concentration of detergent (0.1%) and TMR ligand in phosphate-buffered saline. The cell-free extracts of *E. coli* cells containing DhaA variants (5 μg) were resolved by SDS-PAGE and the densitometric analysis was performed to quantify the amount of target proteins; DhaAHT* 5.3 %, DhaAWT* 7.0 % and DhaA31* 11.2 % of total cellular protein. The binding reaction of the DhaAHT* variant in cell-free extract progressed to completion in a few minutes, as expected, while the binding reaction of cell-free extracts of DhaAWT* and DhaA31* took nearly 10 and 70 hours, respectively (Fig. 7). The determined binding rates of TMR to DhaA variants in cell-free extracts were of the same order of magnitude as those previously obtained for the purified enzymes (Table 4). This indicates that the FP method can be used not only to determine the binding kinetics of purified enzymes, but also for screening of libraries constituted of cell free extracts of enzyme variants with modified tunnels.

Kinetic mechanism of TMR ligand binding to selected DhaA variants

FP binding experiments at various concentrations of TMR were performed with DhaAHT* and DhaA31* variants exhibiting the largest differences in their binding rates (Fig. 8) in order to elucidate whether binding kinetics of studied haloalkane dehalogenases is driven by enzyme-ligand association or by formation of enzyme-probe covalent complex (S_N2 reaction). The kinetic data were globally fitted to a minimal reaction mechanism including (i) association step and (ii) formation of the alkyl-enzyme intermediate (Scheme 1). Kinetic parameters of individual steps of TMR binding to both DhaA variants derived by dynamic kinetic simulation are summarized in Table 5. The confidence contour analysis indicated that estimates of all rate constants are reasonably constrained by kinetic data. Enzyme-ligand association was identified as the slowest step in the kinetic mechanism of TMR binding to both DhaAHT* and DhaA31*. In the case of DhaA31*, the association step was more than five orders of magnitude slower than that of DhaAHT*, explaining dramatic difference in binding efficiency between these two variants. Although the cleavage of carbon-halogen bond leading to the formation of covalent complex (S_N2 step) was significantly faster than enzyme-probe association in the kinetic mechanism of TMR binding to both variants, two orders of magnitude difference in the rate of S_N2 reaction between DhaA31* and DhaAHT* also contributes to a large difference between the variants.

DISCUSSION

The FP method has been successfully exploited in various applications including protein-protein interactions [49], DNA-protein interactions [50], enzyme inhibitor identification [51], enzyme activity [52] and protein-ligand interactions [41]. Our study focused on the utility of FP for determining binding kinetics of fluorescent ligands to DhaA and LinB haloalkane dehalogenase variants with modified access tunnels. For this purpose, we used variants that carry a mutation at the catalytic histidine enabling covalent bonding between HaloTag ligands and their active sites, effectively preventing the reaction proceeding beyond formation of the alkyl-enzyme intermediate [34, 45].

The FP method was sufficiently sensitive to detect and quantify differences in the binding kinetics of tested variants with various access tunnel modifications. The DhaA variants can be ordered according to their binding rate constants as follows: DhaA31* << DhaAWT* < DhaA106* <<< DhaAHT*. The binding rate constant of DhaAHT*, a variant that has a wide tunnel due to introduction of small residues, was seven orders of magnitude higher than that of DhaA31*, which has a sealed access tunnel due to introduction of bulky residues [21]. LinB variants differing in a single amino acid lining the access tunnel were found to have substantially differing binding constants, and the variants could be ordered according to determined binding rate constants as follows: LinBWT* < LinB35* < LinB26*. The increases in binding rate constants of LinB35* and LinB26*, relative to LinBWT*, are due to replacement of a bulky Leu at position 177 by the relatively small substituents Ser and Ala, respectively. No binding of the tested HaloTag ligands to LinB32* and LinB86* was detected, by either FP or MALDI-TOF, presumably due to blockage of the tunnel entrance by introduction of a bulky Trp residue.

The FP experiments revealed that the structure of the ligand's fluorophore moiety strongly affects binding kinetics of the studied haloalkane dehalogenases. For instance, DhaA31* only bound the TMR ligand, and did not appear to interact with the other two fluorescent ligands, Alexa Fluor 488 and R110 direct, at all. MALDI-TOF MS further verified the selectivity of the binding between some of the enzymes and the ligands. Interestingly, there was a difference of 1-2 orders of magnitude between binding constants of TMR and Alexa Fluor 488 to the haloalkane dehalogenase variants. The studied enzymes bound to TMR significantly more rapidly than to Alexa Fluor 488 and R110 direct, confirming the importance of selecting ligands with suitable structures for detailed analysis of the access tunnels of the studied enzymes.

The FP method offers several advantages for monitoring binding kinetics of fluorescent ligands to engineered haloalkane dehalogenases. First, it can detect differences in binding kinetics even when a single point substitution has been introduced into the access tunnel of studied enzyme. For example, it showed that TMR binding constants of the LinB26* and LinB35* variants, which have a single substitution (L177A and L177S, respectively) at the tunnel mouth, are 24- and 5-fold higher, respectively, than those of LinBWT*. Furthermore, the FP experiments were not affected by possible fluorescence quenching due to the close proximity of the ligand's fluorophore moiety to an aromatic residue present at the protein surface of LinB32* and LinB86* variants [48]. MALDI-TOF MS analysis confirmed that neither of these variants can interact with the fluorescent ligands, probably due to closure of the access tunnel by the introduction of a bulky Trp residue [39]. Thus, the FP method can provide fundamental information about enzyme's accessibility to ligands even when little or no detailed structural information is available. The main limitation of this method is the requirement for an introduced mutation at the enzyme's active site that will lead to covalent bonding between the enzyme and a binding ligand (here, the catalytic His).

We also tested the possibility of monitoring binding kinetics of enzymes in cell-free extracts, thereby simplifying the process by avoiding the need to purify the enzymes. For this purpose, we examined the binding kinetics of TMR to DhaA variants in cell-free extracts and found them to be consistent with those of the respective purified enzymes. DhaAHT*, which has been engineered to have a large tunnel opening, bound to TMR most rapidly, followed by DhaAWT* [34]. The variant DhaA31*, which has an occluded active site cavity due to the introduction of bulky residues in both main and slot tunnels [21], bound to TMR most slowly.

The results indicate that differences in tunnel geometry can be monitored directly in cell-free extracts. Thus, the FP method could have applications in the medium-throughput screening of enzyme libraries to identify enzyme variants with optimal tunnel geometries.

FP experiments performed at constant enzyme concentration and various concentrations of the probe followed by dynamic kinetic simulation of the data can provide detailed insight into the kinetics of interactions between the enzyme and the probe. The results gained for DhaAHT* and DhaA31* variants revealed that enzyme-probe association is the slowest step in binding kinetics of TMR to both enzyme variants. Seven orders of magnitude difference between binding efficiency of DhaAHT* and DhaA31* with TMR was attributed mainly to the large disparity in the rate of association step of both enzymes, while less pronounced difference was observed for velocity of the following chemical step. FP method thus holds good potential to reveal detailed information about the binding kinetics of studied enzyme systems.

In summary, the current study utilized haloalkane dehalogenases as model enzymes for real-time monitoring of binding kinetics of HaloTag fluorescent ligands. The determined binding kinetics of haloalkane dehalogenase variants correlate well with the nature of introduced mutations in their access tunnels. The method can elucidate the accessibility of tunnels and active sites in engineered and novel haloalkane dehalogenases, thereby complementing the information about the enzyme structure gained by other biophysical techniques. The presented approach for monitoring binding kinetics can be extended to other enzymes forming covalent alkyl-enzyme intermediate during their catalytic cycle, such as α/β-hydrolases possessing more than 100,000 protein sequences according to the Pfam database, if the suitable fluorescent ligand to conduct such studies is available or can be developed. In general, all α/β-hydrolase enzymes have a nucleophile-base-acid catalytic triad and their reaction mechanism proceeds via a covalent acyl-enzyme intermediate, subsequently cleaved by a water molecule. For binding kinetics analysis, the covalent complex between the suitable fluorescent ligand and enzyme can be monitored by FP method. This method can also be applied to medium-throughput screening of a library constituted of the cell-free extracts of enzyme variants in directed evolution experiments. Furthermore, the method can be conveniently used for identification of rate-determining step in binding kinetics of studied enzymes.

MATERIALS AND METHODS

Materials

All chemicals, media components, and mutagenic oligonucleotides were purchased from Sigma-Aldrich (St. Louis, USA), unless stated otherwise. HaloTag ligands were purchased from Promega Corporation (Madison, USA). DNA and protein molecular weight markers were purchased from Takara (Shiga, Japan). The 96-well black polypropylene plates used in fluorescence polarization measurements were purchased from Nunc (St. Louis, USA).

Construction of haloalkane dehalogenase variants with mutation in catalytic histidine

Mutant recombinant genes were obtained using a QuikChange™ Site-Directed Mutagenesis Kit (Stratagene, Santa Clara, USA) according to the manufacturer's instructions, except for the *dhaAHT* gene, which is commercially available (Promega, Madison, USA). The specific complementary primers designed to encode the substitution H272F in *dhaA* and *linB* recombinant genes are summarized in Table S1. The resulting PCR products were treated with DpnI enzyme to remove the template plasmids and then transformed into XL-1 Blue

super chemocompetent cells (Stratagene, Santa Clara, USA). The nucleotide sequences of all constructed mutants were confirmed by DNA sequencing (GATC, Konstanz, Germany).

Enzyme expression and purification

The constructed genes of *dhaA* and *linB* variants subcloned into the expression vector pAQN and pET21 (Table S1) were transformed into *E. coli* BL21 and BL21(DE3) cells respectively, for protein expression. The cells were grown at 37 °C until they reached an optical density of about 0.6 at 600 nm in Luria-Bertani (LB) medium containing ampicillin (100 μg/ml). The protein expression was induced by addition of 0.5 mM isopropyl β-D-1-thiogalacto-pyranoside and cells were further incubated at 20 °C. After overnight cultivation, the cells were harvested by centrifugation at 3,700 x g for 10 min at 4 °C. During harvesting, the cells were washed with 50 mM potassium phosphate buffer (pH 7.5) containing 10% glycerol, resuspended in equilibrating purification buffer (16.4 mM K_2HPO_4, 3.6 mM KH_2PO_4, 500 mM NaCl, 10 mM imidazole), pH 7.5 and frozen at 80 °C. Defrosted cell suspensions were sonicated in a Hielscher UP200S ultrasonic processor (Hielscher, Teltow, Germany). Cell debris was removed by centrifugation at 21,000 x g for 1 hour at 4 °C. The crude extract was collected, filtered and applied on Ni-NTA Superflow Cartridge (Qiagen, Hilden, Germany) which was equilibrated with purification buffer (16.4 mM K_2HPO_4, 3.6 mM KH_2PO_4, 500 mM NaCl, 10 mM imidazole), pH 7.5. C-terminus His-tagged enzymes were eluted using purification buffer containing 300 mM imidazole. The eluted proteins were dialyzed against phosphate-buffered saline (PBS: 137 mM NaCl, 2.7 mM KCl, 10 mM Na_2HPO_4, 1.8 mM KH_2PO_4), pH 7.4. Protein concentrations were measured using the Bradford protein assay with bovine serum albumin as a standard. The protein purity was confirmed by SDS-polyacrylamide gel electrophoresis (SDS-PAGE) using 15% polyacrylamide gels, stained with Coomassie brilliant blue R-250 dye (Fluka, Buchs, Switzerland).

Circular dichroism (CD) spectroscopy

CD spectra of the studied enzymes were recorded at 20 °C using a Chirascan spectropolarimeter (Applied Photophysics, Surrey, United Kingdom) equipped with a Peltier thermostat. Data were collected from 185 to 260 nm, at 100 nm/min, with a 1 s response time and 2 nm bandwidth. The enzyme samples were placed in a 0.1 cm quartz cuvette, at a concentration of 0.2 mg/ml. The spectrum of each studied enzyme is presented as an average of five individual scans and was corrected for buffer absorbance. The obtained spectrum curves were smoothed with a Savitsky-Golay filter [53]. CD data were expressed in terms of the mean residue ellipticity (Θ_{MRE}) using Eq. 1:

$$\Theta_{MRE} = \frac{\Theta_{obs} M_w 100}{n c l} \quad (1)$$

where Θ_{obs} is the observed ellipticity in degrees, M_w is the molecular weight of the protein, n is number of residues, l is the cell path length, c is the protein concentration and the factor 100 is required for converting molecular weight to mg/dmol.

Fluorescence polarization for quantifying binding kinetics

Fluorescence polarization measurements were performed at room temperature using an Infinite F500 plate reader (Tecan, Männedorf, Switzerland) equipped with required polarizers for excitation and emission. The purified haloalkane dehalogenases with modified access tunnels and additional H272F substitution were reacted with selected HaloTag ligands in PBS containing 0.01% CHAPS detergent to minimize non-specific interactions. The concentrations of the selected haloalkane dehalogenases were usually in excess against the

fixed concentration of employed HaloTag ligands: Alexa Fluor 488 (0.075 µM), TMR and R110 direct (both at 0.01 µM). Ligand binding was monitored by changes in fluorescence polarization over time. Simultaneously the fluorescence polarization of the free probe in buffer was also monitored. The excitation and emission wavelengths were set to 485 and 535 nm, respectively, for Alexa Fluor 488, and to 544 and 580 nm, respectively, for both R110 direct and TMR ligands. The FP experiments with cell-free extracts were performed as described above, except that the concentration of CHAPS detergent (0.1%) was higher in the reaction mixture. Origin 8.0 software (OriginLab, Northampton, USA) was used to determine apparent rate constants by nonlinear curve fitting of the experimental data to kinetic models describing either pseudo-first order (Eq. 2) or second order (Eq. 3) rates:

$$\ln\frac{[A_0]}{[A]} = k\,\mathrm{t} \quad (2)$$

$$\ln\frac{[B][A_0]}{[A][B_0]} = k([B_0]-[A_0])\,\mathrm{t} \quad (3)$$

where k is the rate constant, B_0 and A_0 are the reactant concentrations at time = 0, and B and A are concentrations of the reactants at time = t. To convert the calculated pseudo first order rate constants to apparent second order rate constants, they were divided by the concentration of the reactant in excess.

Kinetic analysis of TMR binding to selected DhaA variants

The binding of TMR ligand to DhaAHT* and DhaA31* was monitored by changes in fluorescence polarization over time. The time courses of fluorescence polarization measured at different concentrations of TMR probe were simultaneously fitted to the kinetic model describing minimal two-step binding mechanism by using dynamic kinetic simulation program KinTek Global Kinetic Explorer version 4.0 (KinTek, Snow Shoe, USA):

Scheme 1 here

Here E is enzyme, L is TMR ligand, E.L is enzyme-ligand complex, E-L is covalently bound enzyme-ligand complex, k_{assoc} and k_{dissoc} is rate of enzyme-ligand complex formation and dissociation, respectively, and k_{SN2} is rate of the chemical step (S_N2) leading to covalently trapped enzyme-ligand complex. During data fitting based on numerical integration of rate equations from an input model, the program sought parameters that resulted in the minimum χ^2 value using nonlinear regression based on the Levenberg-Marquardt method. The standard error (SE) was calculated from the covariance matrix during nonlinear regression for global fitting of all polarization traces for each binding experiment [54]. Estimate for the enzyme-ligand dissociation constant was derived as follows: $K_{eq} = k_{dissoc}/k_{assoc}$.

MALDI-TOF MS analysis

To check whether or not the haloalkane dehalogenases with modified tunnels form covalent linkages with the ligands, MALDI-TOF MS was used as follows. Phosphate buffer used for purification of haloalkane dehalogenases with modified tunnels was exchanged with glycine buffer (20 mM, pH 8.6) by overnight dialysis. The protein-ligand reaction proceeded in a volume of 100 µl at room temperature. Concentration of the enzyme was 1 mg/ml and

concentration of the ligand was adjusted to achieve 100% saturation of the enzyme. MALDI-TOF mass spectra were recorded on an Ultraflextreme instrument (Bruker Daltonics, Billerica, Germany) operated in linear mode for detecting positive ions. Ferulic acid (12.5 mg/mL in a mixture of water:acetonitrile:formic acid 50:33:17, v/v/v) was used as the MALDI matrix. 0.6 µl of the enzyme sample was mixed with 2.4 µl of matrix solution, after which 0.6 µl of the mixture was deposited onto a stainless steel MALDI target. Protein Calibration mixture II (Bruker Daltonics, Billerica, Germany) was used for external calibration of the mass spectra, which were processed with FlexAnalysis 3.4 software (Bruker Daltonics, Billerica,Germany).

ACKNOWLEDGEMENTS

This work was supported by the Grant Agency of the Czech Republic (grant no. P207/12/0775), Grant of the Ministry of Education of Czech Republic (grant nos. LO1214, LH14027 and LQ1605), and Internal Grant Agency of Masaryk University (grant no. MUNI/M/1888/2014). SK was supported by the "Employment of Best Young Scientists for International Cooperation Empowerment" project (CZ.1.07/2.3.00/30.0037), co-financed by the European Social Fund and the state budget of the Czech Republic.

AUTHOR CONTRIBUTIONS

S.K., Z.P., J.D. and R.C. designed experiments; S.K. performed experiments; S.K., Z.P. and R.C. interpreted data; S.K., Z.P., J.D. and R.C. wrote the manuscript.

REFERENCES

1. Raushel FM, Thoden JB & Holden HM (2003) Enzymes with molecular tunnels. *Acc Chem Res* **36**, 539-548.
2. Ericsson DJ, Kasrayan A, Johansson P, Bergfors T, Sandström AG, Bäckvall JE & Mowbray SL (2008) X-ray Structure of *Candida antarctica* Lipase A shows a novel lid structure and a likely mode of interfacial activation. *J Mol Biol* **376**, 109-119.
3. Uppenberg J, Oehrner N, Norin M, Hult K, Kleywegt GJ, Patkar S, Waagen V, Anthonsen T & Jones TA (1995) Crystallographic and molecular-modeling studies of lipase B from *Candida antarctica* reveal a stereospecificity pocket for secondary alcohols. *Biochemistry* **34**, 16838-16851.
4. Pleiss J, Fischer M & Schmid RD (1998) Anatomy of lipase binding sites: the scissile fatty acid binding site. *Chem Phys Lipids* **93**, 67-80.
5. Nardini M, Ridder IS, Rozeboom HJ, Kalk KH, Rink R, Janssen DB & Dijkstra BW (1999) The X-ray Structure of Epoxide Hydrolase from *Agrobacterium radiobacter* AD1 an enzyme to detoxify harmful epoxides. *J Biol Chem* **274**, 14579-14586.
6. Kotik M, Stepanek V, Kyslík P & Maresova H (2007) Cloning of an epoxide hydrolase-encoding gene from *Aspergillus niger* M200, overexpression in *E. coli*, and modification of activity and enantioselectivity of the enzyme by protein engineering. *J Biotechnol* **132**, 8-15.
7. Oakley AJ, Klvana M, Otyepka M, Nagata Y, Wilce MC & Damborsky J (2004) Crystal structure of haloalkane dehalogenase LinB from *Sphingomonas paucimobilis* UT26 at 0.95 Å resolution: dynamics of catalytic residues. *Biochemistry* **43**, 870-878.
8. Klvana M, Pavlova M, Koudelakova T, Chaloupkova R, Dvorak P, Prokop Z, Stsiapanava A, Kuty M, Kuta-Smatanova I & Dohnalek J (2009) Pathways and mechanisms for product release in the engineered haloalkane dehalogenases explored

using classical and random acceleration molecular dynamics simulations. *J Mol Biol* **392**, 1339-1356.
9. Petrek M, Otyepka M, Banas P, Kosinova P, Koca J & Damborsky J (2006) CAVER: a new tool to explore routes from protein clefts, pockets and cavities. *BMC Bioinformatics* **7**, 316.
10. Hyde C, Ahmed S, Padlan E, Miles EW & Davies D (1988) Three-dimensional structure of the tryptophan synthase alpha 2 beta 2 multienzyme complex from *Salmonella typhimurium*. *J Biol Chem* **263**, 17857-17871.
11. Kim J & Raushel FM (2004) Access to the carbamate tunnel of carbamoyl phosphate synthetase. *Arch Biochem Biophys* **425**, 33-41.
12. Wang LK, Lima CD & Shuman S (2002) Structure and mechanism of T4 polynucleotide kinase: an RNA repair enzyme. *EMBO J* **21**, 3873-3880.
13. Wilce MC, Dooley DM, Freeman HC, Guss JM, Matsunami H, McIntire WS, Ruggiero CE, Tanizawa K & Yamaguchi H (1997) Crystal structures of the copper-containing amine oxidase from *Arthrobacter globiformis* in the holo and apo forms: implications for the biogenesis of topaquinone. *Biochemistry* **36**, 16116-16133.
14. Wade RC, Winn PJ & Schlichting I (2004) A survey of active site access channels in cytochromes P450. *J Inorg Biochem* **98**, 1175-1182.
15. Wagner U, Hasslacher M, Griengl H, Schwab H & Kratky C (1996) Mechanism of cyanogenesis: the crystal structure of hydroxynitrile lyase from *Hevea brasiliensis*. *Structure* **4**, 811-822.
16. May M, Mehboob S, Mulhearn DC, Wang Z, Yu H, Thatcher GR, Santarsiero BD, Johnson ME & Mesecar AD (2007) Structural and functional analysis of two glutamate racemase isozymes from *Bacillus anthracis* and implications for inhibitor design. *J Mol Biol* **371**, 1219-1237.
17. Damborsky J, Chaloupkova R, Pavlova M, Chovancova E & Brezovsky J (2010) Structure–function relationships and engineering of haloalkane dehalogenases. In *Handbook of Hydrocarbon and Lipid Microbiology* (Timmis KN, ed), pp. 1081-1098, Springer, Berlin.
18. Damborsky J & Brezovsky J (2009) Computational tools for designing and engineering biocatalysts. *Curr Opin Chem Biol* **13,** 26-34.
19. Brezovsky J, Chovancova E, Gora A, Pavelka A, Biedermannova L & Damborsky J (2013) Software tools for identification, visualization and analysis of protein tunnels and channels. *Biotechnol Adv* **31**, 38-49.
20. Prokop Z, Gora A, Brezovsky J, Chaloupkova R, Stepankova V & Damborsky J (2012) Engineering of Protein Tunnels: The keyhole–lock–key model for catalysis by enzymes with buried active sites. In *Protein Engineering Handbook* (Lutz S & Bornscheuer UT, eds), pp 421-464, Wiley-VCH, Weinheim.
21. Pavlova M, Klvana M, Prokop Z, Chaloupkova R, Banas P, Otyepka M, Wade RC, Tsuda M, Nagata Y & Damborsky J (2009) Redesigning dehalogenase access tunnels as a strategy for degrading an anthropogenic substrate. *Nature Chem Biol* **5**, 727-733.
22. Koudelakova T, Chaloupkova R, Brezovsky J, Prokop Z, Sebestova E, Hesseler M, Khabiri M, Plevaka M, Kulik D & Kuta Smatanova I (2013) Engineering enzyme stability and resistance to an organic cosolvent by modification of residues in the access tunnel. *Angew Chem Int Ed* **52**, 1959-1963.
23. Ba L, Li P, Zhang H, Duan Y & Lin Z (2013) Semi-rational engineering of cytochrome P450sca-2 in a hybrid system for enhanced catalytic activity: Insights into the important role of electron transfer. *Biotechnol Bioeng* **110**, 2815-2825.

24. Schmitt J, Brocca S, Schmid RD & Pleiss J (2002) Blocking the tunnel: engineering of *Candida rugosa* lipase mutants with short chain length specificity. *Protein Eng* **15**, 595-601.
25. Lafaquiere V, Barbe S, Puech-Guenot S, Guieysse D, Cortes J, Monsan P, Simeon T, Andre I & Remaud-Simeon M (2009) Control of lipase enantioselectivity by engineering the substrate binding site and access channel. *ChemBioChem* **10**, 2760-2771.
26. Kopecny D, Tylichova M, Snegaroff J, Popelkova H & Sebela M (2011) Carboxylate and aromatic active-site residues are determinants of high-affinity binding of ω-aminoaldehydes to plant aminoaldehyde dehydrogenases. *FEBS J* **278**, 3130-3139.
27. Sandstrom AG, Wikmark Y, Engstrom K, Nyhlen J & Backvall JE (2012) Combinatorial reshaping of the *Candida antarctica* lipase A substrate pocket for enantioselectivity using an extremely condensed library. *Proc Natl Acad Sci* **109**, 78-83.
28. Wittrup Larsen M, Zielinska DF, Martinelle M, Hidalgo A, Jensen L J, Bornscheuer UT & Hult K (2010) Suppression of water as a nucleophile in *Candida antarctica* lipase B catalysis. *ChemBioChem* **11**, 796-801.
29. Syren PO, Hammer SC, Claasen B & Hauer B (2014) Entropy is key to the formation of pentacyclic terpenoids by enzyme-catalyzed polycyclization. *Angew Chem Int Ed* **126**, 4945-4949.
30. Stucki G & Thueer M (1995) Experiences of a large-scale application of 1, 2-dichloroethane degrading microorganisms for groundwater treatment. *Environ Sci & Technol* **29**, 2339-2345.
31. Bidmanova S, Chaloupkova R, Damborsky J & Prokop Z (2010) Development of an enzymatic fiber-optic biosensor for detection of halogenated hydrocarbons. *Anal Bioanal Chem* **398**, 1891-1898.
32. Westerbeek A, Szymanski W, Feringa BL & Janssen DB (2011) Dynamic kinetic resolution process employing haloalkane dehalogenase. *ACS Catal* **1**, 1654-1660.
33. Koudelakova T, Bidmanova S, Dvorak P, Pavelka A, Chaloupkova R, Prokop Z. & Damborsky J (2013) Haloalkane dehalogenases: biotechnological applications. *Biotechnol J* **8**, 32-45.
34. Los GV, Encell LP, McDougall MG, Hartzell DD, Karassina N, Zimprich C, Wood MG, Learish R, Ohana RF & Urh M (2008) HaloTag: a novel protein labeling technology for cell imaging and protein analysis. *ACS Chem Biol* **3**, 373-382.
35. Kulakova AN, Larkin MJ & Kulakov LA (1997) The plasmid-located haloalkane dehalogenase gene from *Rhodococcus rhodochrous* NCIMB 13064. *Microbiology* **143**, 109-115.
36. Nagata Y, Miyauchi K, Damborsky J, Manova K, Ansorgova A & Takagi M (1997) Purification and characterization of a haloalkane dehalogenase of a new substrate class from a gamma-hexachlorocyclohexane-degrading bacterium, *Sphingomonas paucimobilis* UT26. *Appl Environ Microbiol* **63**, 3707-3710.
37. Damborsky J, Prokop Z, Koudelakova T, Stepankova V, Chaloupkova R, Chovancova E, Gora AW & Brezovsky J (2013) Method of thermostabilization of a protein and/or stabilization towards organic solvents. Patent US 8580932 B2.
38. Liskova V, Bednar D, Prudnikova T, Rezacova P, Koudelakova T, Sebestova E, Smatanova IK, Brezovsky J, Chaloupkova R & Damborsky J (2015) Balancing the stability–activity trade-off by fine-tuning dehalogenase access tunnels. *ChemCatChem* **7**, 648-659.
39. Chaloupkova R, Sykorova J, Prokop Z, Jesenska A, Monincova M, Pavlova M, Tsuda M, Nagata Y & Damborsky J (2003) Modification of activity and specificity of haloalkane dehalogenase from *Sphingomonas paucimobilis* UT26 by engineering of its entrance tunnel. *J Biol Chem* **278**, 52622-52628.

40. Perrin F (1926) Polarization of light of fluorescence, average life of molecules in the excited state. *J Phys Radium* **7**, 390-401.
41. Rossi AM & Taylor CW (2011) Analysis of protein-ligand interactions by fluorescence polarization. *Nat Protoc* **6**, 365-387.
42. Lea WA & Simeonov A (2011) Fluorescence polarization assays in small molecule screening. *Expert Opin Drug Discov* **6**, 17-32.
43. Owicki JC (2000) Fluorescence polarization and anisotropy in high throughput screening: perspectives and primer. *J Biomol Screen* **5**, 297-306.
44. Prokop Z, Monincova M, Chaloupkova R, Klvana M, Nagata Y, Janssen DB & Damborsky J (2003) Catalytic mechanism of the haloalkane dehalogenase LinB from *Sphingomonas paucimobilis* UT26. *J Biol Chem* **278**, 45094-45100.
45. Pieters RJ, Fennema M, Kellogg RM & Janssen DB (1999) Design and synthesis of reagents for phage display screening of dehalogenases. *Bioorg Med Chem Lett* **9**, 161-166.
46. Venyaminov SY & Yang JT (1996) Determination of protein secondary structure. In *Circular dichroism and the conformational analysis of biomolecules* (Fasman GD, ed), pp 69-107, Plenum Press, New York.
47. Encell LP, Ohana RF, Zimmerman K, Otto P, Vidugiris G, Wood MG, Los GV, McDougall MG, Zimprich, C & Karassina N (2012) Development of a dehalogenase-based protein fusion tag capable of rapid, selective and covalent attachment to customizable ligands. *Curr Chem Genom* **6**, 55.
48. Pospisil P, Luxem KE, Ener M, Sykora J, Kocabova J, Gray HB, Vlcek Jr An & Hof M (2014) Fluorescence quenching of (dimethylamino) naphthalene dyes badan and prodan by tryptophan in cytochromes P450 and micelles. *J Phys Chem B* **118**, 10085-10091.
49. Jameson DM & Seifried SE (1999) Quantification of protein–protein interactions using fluorescence polarization. *Methods* **19**, 222-233.
50. Chan C, Wu Z, Ciardelli T, Eastman A & Bresnick E (1993) Kinetic and DNA-binding properties of recombinant human O 6-methylguanine-DNA methyltransferase. *Arch Biochem Biophys* **300**, 193-200.
51. Baughman BM, Jake Slavish P, DuBois RM, Boyd VA, White SW & Webb TR (2012) Identification of influenza endonuclease inhibitors using a novel fluorescence polarization assay. *ACS Chem Biol* **7**, 526-534.
52. Bolger R & Checovich W (1994) A new protease activity assay using fluorescence polarization. *BioTechniques* **17**, 585-589.
53. Savitzky A & Golay MJ (1964) Smoothing and differentiation of data by simplified least squares procedures. *Anal Chem* **36**, 1627-1639.
54. Johnson KA, Simpson ZB & Blom T (2009) Global kinetic explorer: a new computer program for dynamic simulation and fitting of kinetic data. *Anal Biochem* **387**, 20-29.
55. Nagata Y, Miyauchi K & Takagi M (1999) Complete analysis of genes and enzymes for γ-hexachlorocyclohexane degradation in *Sphingomonas paucimobilis* UT26. *J Ind Microbiol Biotechnol* **23**, 380-390.
56. Kellogg EH, Leaver-Fay A & Baker D (2011) Role of conformational sampling in computing mutation-induced changes in protein structure and stability. *Proteins: Struct, Funct, Bioinfo* **79**, 830-838.

SUPPORTING INFORMATION

Table S1. Oligonucleotides used for site-directed mutagenesis.

TABLES

Table 1. List of haloalkane dehalogenases with descriptions of enzyme properties and access tunnel geometries.

Enzyme	Mutations	Enzyme properties	References
DhaAWT*	H272F	DhaAWT is involved in the degradation of environmental pollutants such as chlorinated alkanes. The enzyme has a buried active site connected to the surrounding solvent by a main and slot tunnels. Preferred substrates are terminally and vicinally halogenated compounds with chain length of C2-C10 carbon atoms.	[17]
DhaAHT* (HaloTag)	K175M C176G Y273L H272F	DhaA variant with access tunnel fine-tuned by site saturation mutagenesis to enable HaloTag ligands to access the binding site easily. The determined binding rate of the enzyme to a TMR ligand is comparable to the rate in the strongest known non-covalent interaction, the biological interaction between streptavidin and biotin.	[34, 47]
DhaA31*	I135F C176Y V245F L246I Y273F H272F	This DhaA variant has a 32-fold higher catalytic activity towards the anthropogenic compound 1,2,3-trichloropropane than DhaAWT. Bulky residues have been introduced to this variant's tunnel, which occludes the active site cavity.	[21]
DhaA106*	T148L G171Q A172V F176G H272F	DhaA variant with balanced catalytic activity, thermostability and resistance towards organic co-solvents. The F176G substitution at the tunnel entrance facilitated its opening and enhanced mobility of α-helices lining the access tunnel.	[38]
LinBWT*	H272F	LinBWT participates in degradation of the insecticide γ-hexachlorocyclohexane. The active site is buried in the protein interior and is connected with surrounding solvent by the main and slot tunnels, which are less accessible to the solvent compared to DhaAWT. Preferred substrates include terminally, vicinally, β-halogenated and cyclic compounds with chain length C2-C10 carbon atoms.	[17, 55]

LinB26*	L177A H272F	This LinB variant includes a substitution of residue Leu177 for the small non-polar amino acid Ala and increased enzymatic activity towards selected substrates, probably due to the consequent change in amino acid size and polarity at the access tunnel mouth.	[39]
LinB35*	L177S H272F	In this LinB variant the Leu177 has been replaced by the small polar amino acid Ser, decreasing enzymatic activity towards selected substrates. Polar residues in the tunnel mouth did not favor the binding of substrate molecules to enzyme active site.	[39]
LinB32*	L177W H272F	In this variant exchange of Leu177 at the tunnel mouth for the bulky and hydrophobic Trp effectively blocks access to the tunnel, causing a dramatic drop in enzyme activity towards the tested halogenated substrates.	[39]
LinB86*	L177W W140A F143L I211L H272F	This LinB variant was derived from the LinB32 mutant exhibiting closed main access tunnel and newly introduced auxiliary access tunnel. The variant shows enhanced catalytic activity with a large number of halogenated compounds.	Submitted for publication

*Star symbol refers to H272F mutation introduced for trapping of the covalent alkyl-enzyme intermediate.

Table 2. Apparent second order rate constants for binding of two different HaloTag ligands to haloalkane dehalogenase DhaA and LinB with modified access tunnels.

	Apparent second order binding rate constants[a] (M^{-1} s^{-1})	
	Alexa Fluor 488	**TMR**
Enzyme	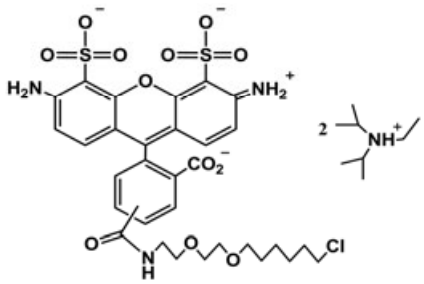	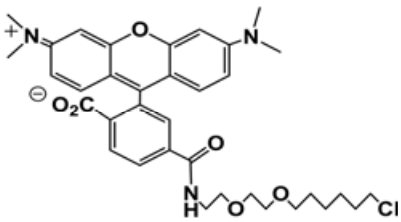
DhaAWT*	1.54 ± 0.16	56.70 ± 2.3
DhaAHT*	0.48 x 10^4 ± 0.03 x 10^4	3.80 x 10^6 ± 0.14 x 10^6
DhaA31*	No binding	0.39 ± 0.01
DhaA106*	80.86 ± 8.1	506.60 ± 6.29
LinBWT*	0.35 ± 0.05	4.60 ± 0.06

LinB26*	1.13 ± 0.16	112.16 ± 13.90
LinB35*	0.42 ± 0.05	23.15 ± 4.50
LinB32*	No binding	No binding
LinB86*	No binding	No binding

[a]Rate constants were measured at room temperature in phosphate-buffered saline, pH 7.4.

Table 3. Apparent second order rate constants for reaction of HaloTag ligand R110 direct with haloalkane dehalogenases with modified tunnels.

Enzyme	**R110 direct and binding constants (M^{-1} s^{-1})**
	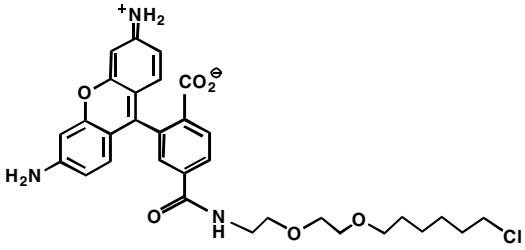
DhaAWT*	-[a]
DhaAHT*	-[a]
DhaA31*	No binding
DhaA106*	484.16 ± 96.8
LinBWT*	-[a]
LinB26*	56.87 ± 3.73
LinB35*	8.75 ± 2.61
LinB32*	-[a]
LinB86*	No binding

[a]Not tested.

Table 4. Apparent rate constants for binding between TMR ligand and DhaA variants in cell-free extracts and the purified variants.

Enzyme	**Apparent second order binding rate constant (M^{-1} s^{-1})**	
	Cell-free extract	**Pure enzymes**
DhaAWT*	11.82	56.7
DhaAHT*	1.39×10^6	3.80×10^6
DhaA31*	0.24	0.39

Table 5. Kinetic constants for binding of TMR ligand to DhaAHT* and DhaA31* determined by dynamic kinetic simulation recorded upon mixing the enzyme with various concentration of the probe.

Enzyme	k_{assoc} ($nM^{-1}.min^{-1}$)	k_{dissoc} (min^{-1})	K_{eq} (nM)	k_{SN2} (min^{-1})
DhaAHT*	0.03 ± 0.01	0.6 ± 0.3	22	0.7 ± 0.4
DhaA31*	$1.4 \pm 0.2 \times 10^{-6}$	0.039 ± 0.007	27850	0.009 ± 0.001

k_{assoc} is rate of enzyme-ligand complex association; k_{dissoc} is rate of enzyme-ligand complex dissociation; k_{SN2} is rate of the S_N2 chemical step leading to covalently trapped enzyme-ligand complex. Standard error was calculated from the covariance matrix during nonlinear regression.

SCHEME

$$E + L \underset{k_{dissoc}}{\overset{k_{assoc}}{\rightleftharpoons}} E.L \xrightarrow{k_{SN2}} E\text{-}L$$

Scheme 1. Two-step binding mechanism for the reaction of TMR with DhaA31* and DhaAHT*.

FIGURE LEGENDS

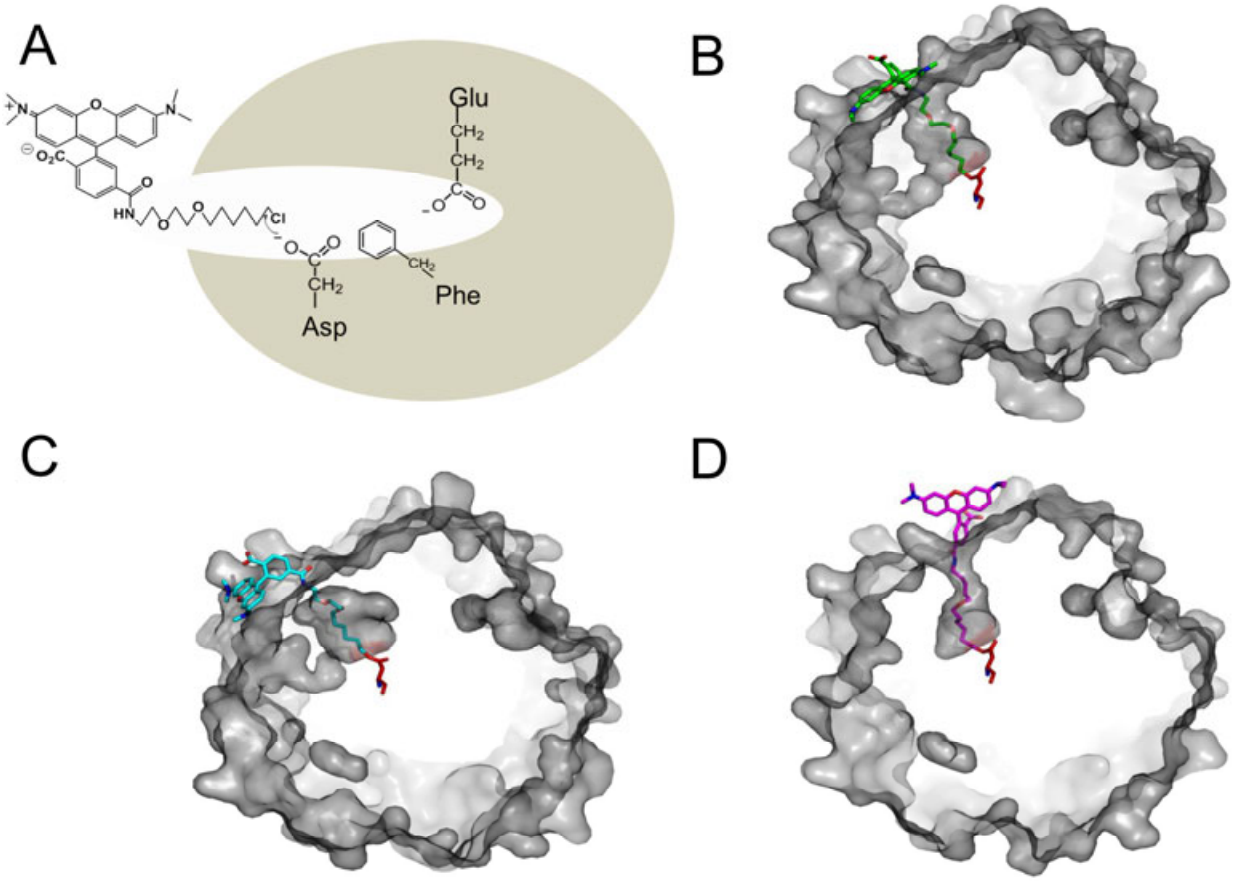

Figure 1. Schematic representation of the formation of covalent ligand-protein complex between the mutants of haloalkane dehalogenase DhaA and the HaloTag TMR ligand (A). Nucleophilic attack by the carboxylate oxygen of Asp on a carbon atom to which a halogen is bound results in the formation of an alkyl-enzyme intermediate. In the wild-type enzyme, catalytic His activates a water molecule to hydrolyze this intermediate. In the mutant enzyme, introduced Phe cannot further afford the hydrolysis of the alkyl-enzyme intermediate, leading to trapped covalent complex. Structural representation of haloalkane dehalogenase DhaAWT* (B), DhaAHT* (C) and DhaA31* (D) covalently linked to TMR ligand, depicting differences in access tunnel geometry of the enzyme variants. The structural models of enzyme-ligand complexes were prepared by the molecular docking of TMR ligand to the respective enzyme variants constructed from the crystal structures of DhaAWT (PDB-ID 4E46) and DhaA31 (PDB-ID 3RK4) using Rosetta [56].

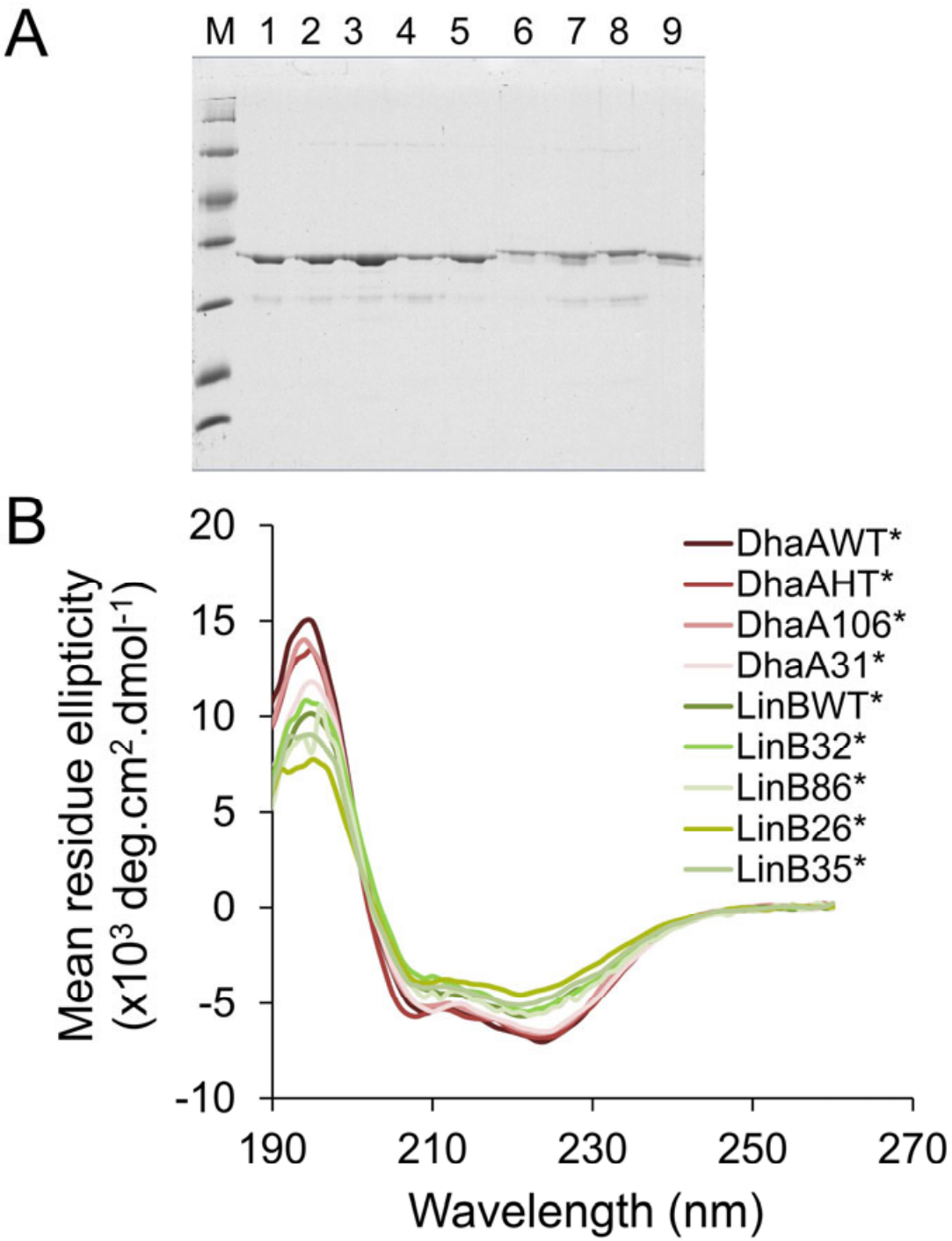

Figure 2. SDS-PAGE (A) and far-UV CD spectra (B) of purified haloalkane dehalogenases with modified tunnels. Lane 1: LinB32*, Lane 2: LinBWT*, Lane 3: LinB86*, Lane 4: LinB26*, Lane 5: LinB35*, Lane 6: DhaAHT*, Lane 7: DhaAWT*, Lane 8: DhaA106*, Lane 9: DhaA31*, M: Protein marker.

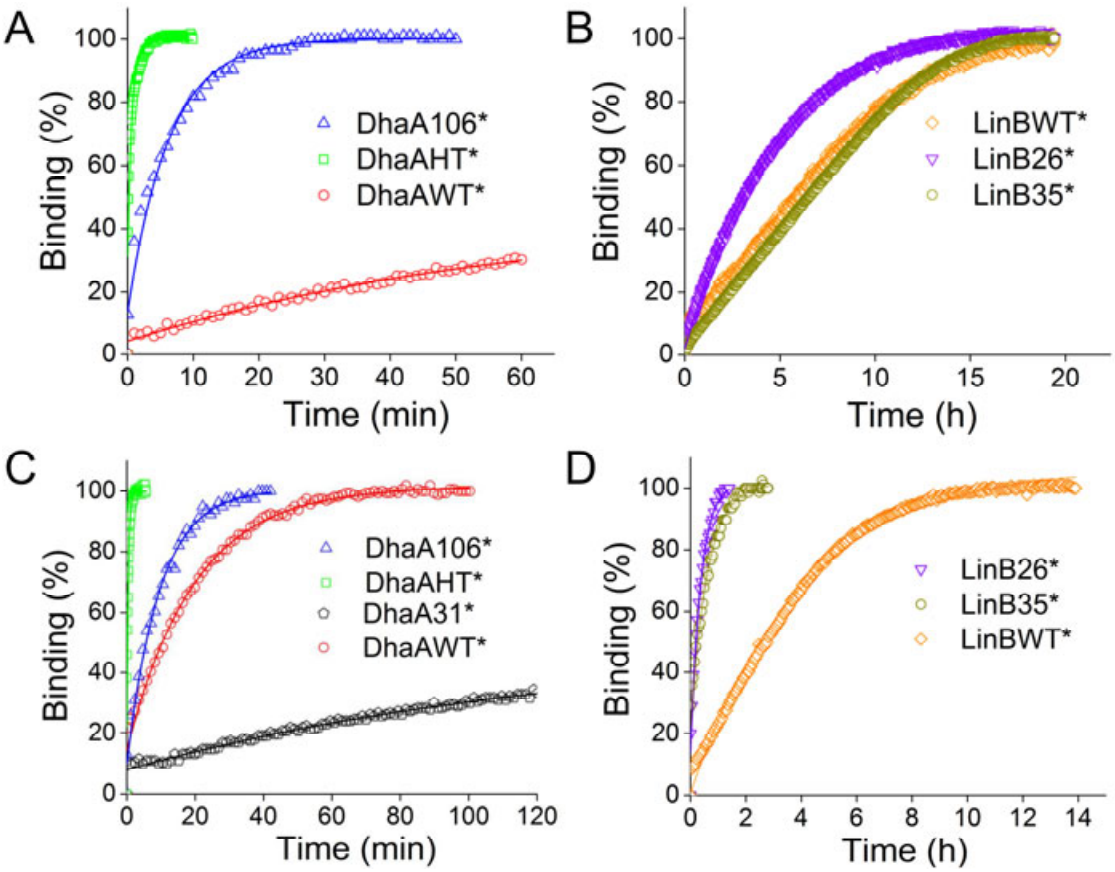

Figure 3. Binding kinetics of fluorescent ligands to haloalkane dehalogenases with modified access tunnels. Binding kinetics of Alexa Fluor 488 to DhaA (A) and LinB (B) variants and binding kinetics of TMR to DhaA (C) and LinB (D) variants.

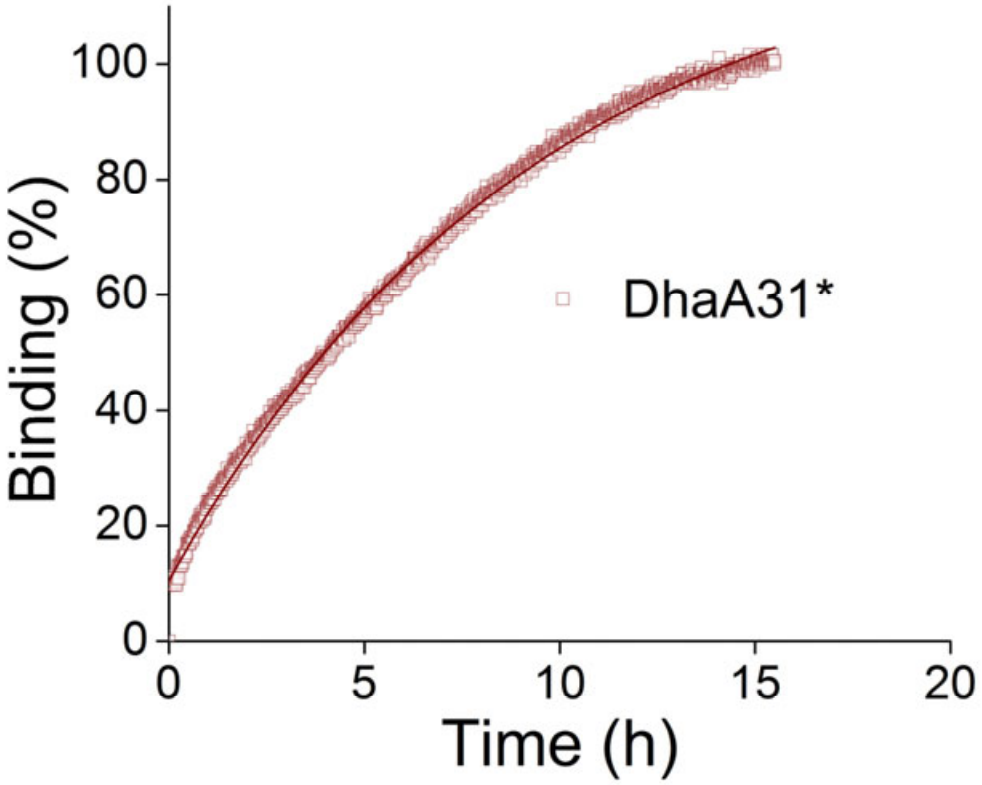

Figure 4. Binding kinetics of TMR ligand to haloalkane dehalogenase DhaA31*.

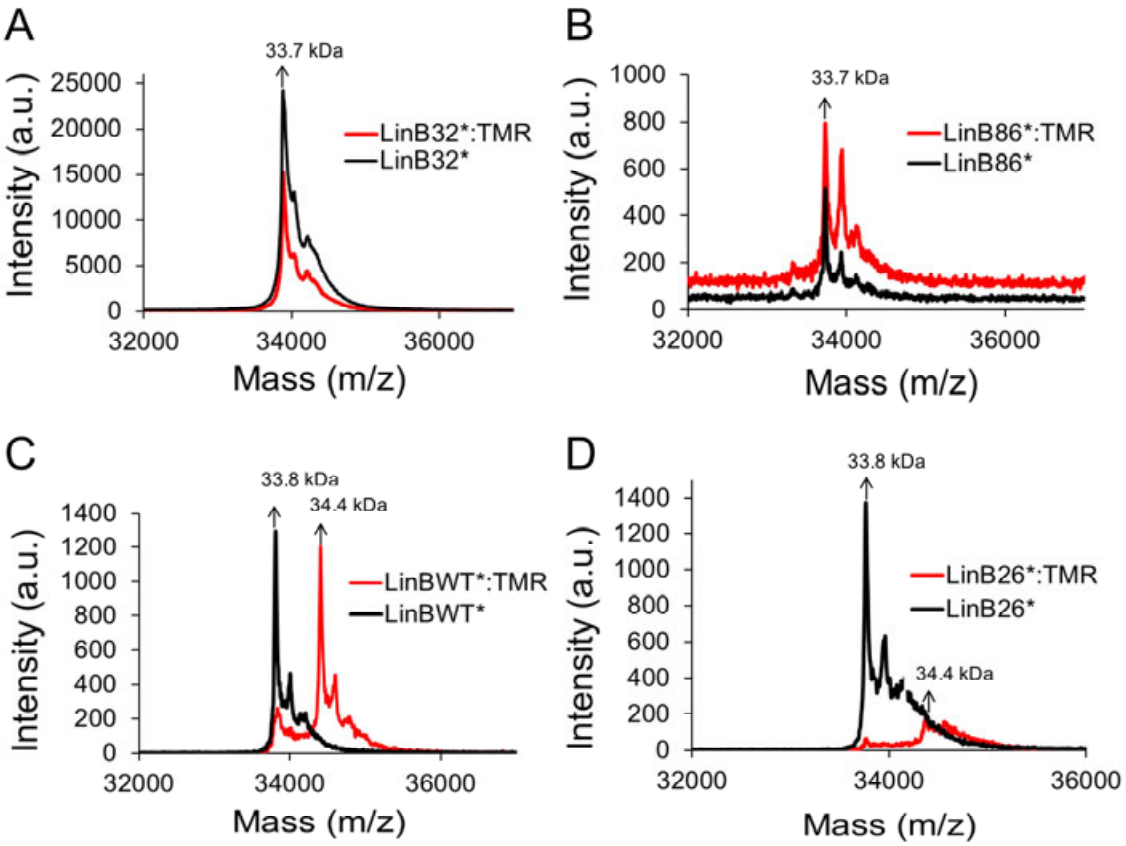

Figure 5. Comparison of MALDI-TOF MS spectra of haloalkane dehalogenase LinB variants LinB32* (A), LinB86* (B), LinBWT* (C) and LinB26* (D) in a free forms and upon their mixing with TMR. The peaks at 34.03 and 34.2 kDa observed in LinB32* spectra most likely corresponds to adducts of protein with gentisic acid (Mw = 154), which was used as MALDI matrix. The peaks at 33.9 and 34.1 kDa observed in LinB86* spectra most likely corresponds to adduct of the protein with ferulic acid (Mw =194 kDa), which was used as MALDI matrix. The peaks at 34.0, 34.4 and 34.6 kDa observed in LinBWT* spectra most likely correspond to adducts of the protein with ferulic acid, which was used as MALDI matrix. Despite the lower quality of LinB26* MS spectra, the modification of the enzyme by TMR ligand is visible. The peaks at 34 kDa observed in LinB26* spectrum most likely correspond to adducts of the protein with ferulic acid which was used as MALDI matrix.

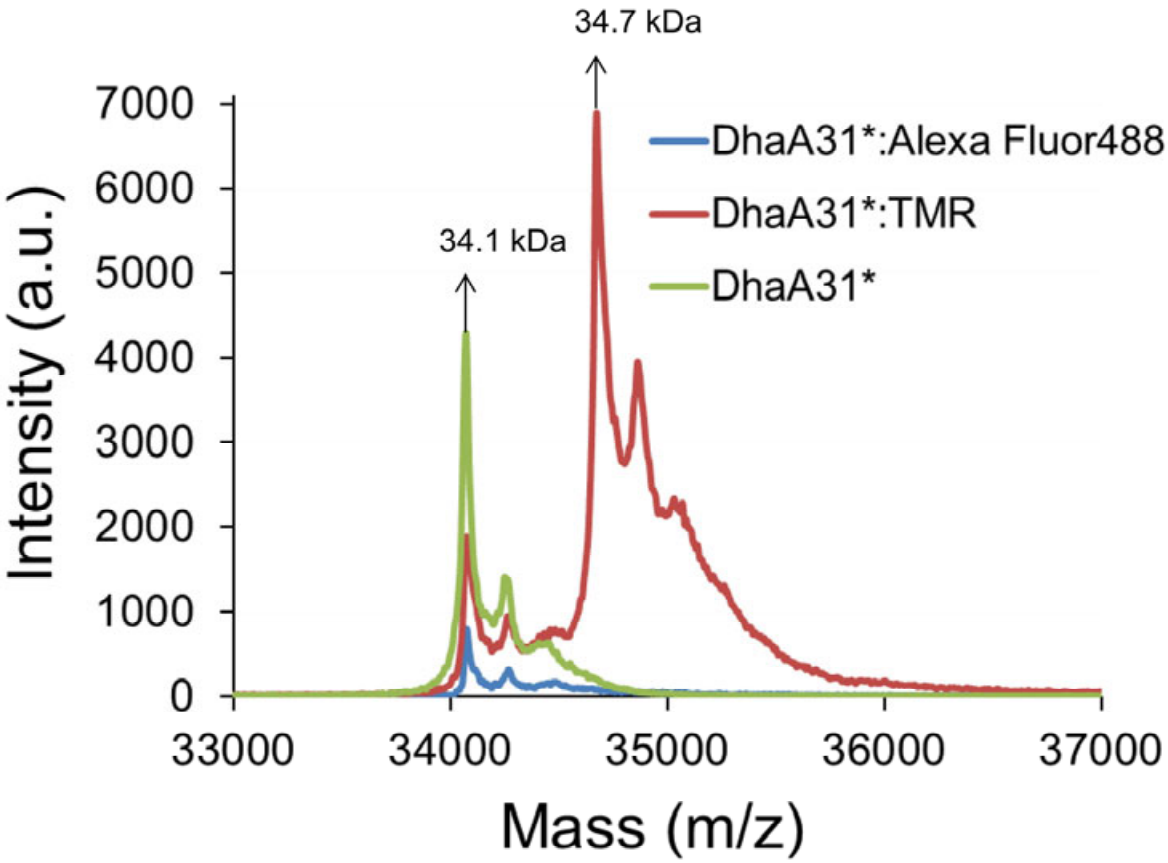

Figure 6. MALDI-TOF MS spectra of DhaA31* enzyme, in free form and in solution with HaloTag ligands Alexa Fluor 488 and TMR. The peaks at 34.2 kDa and 34.8 kDa probably correspond to adducts formed by the reaction of protein with ferulic acid (Mw =194 kDa) which was used as MALDI matrix.

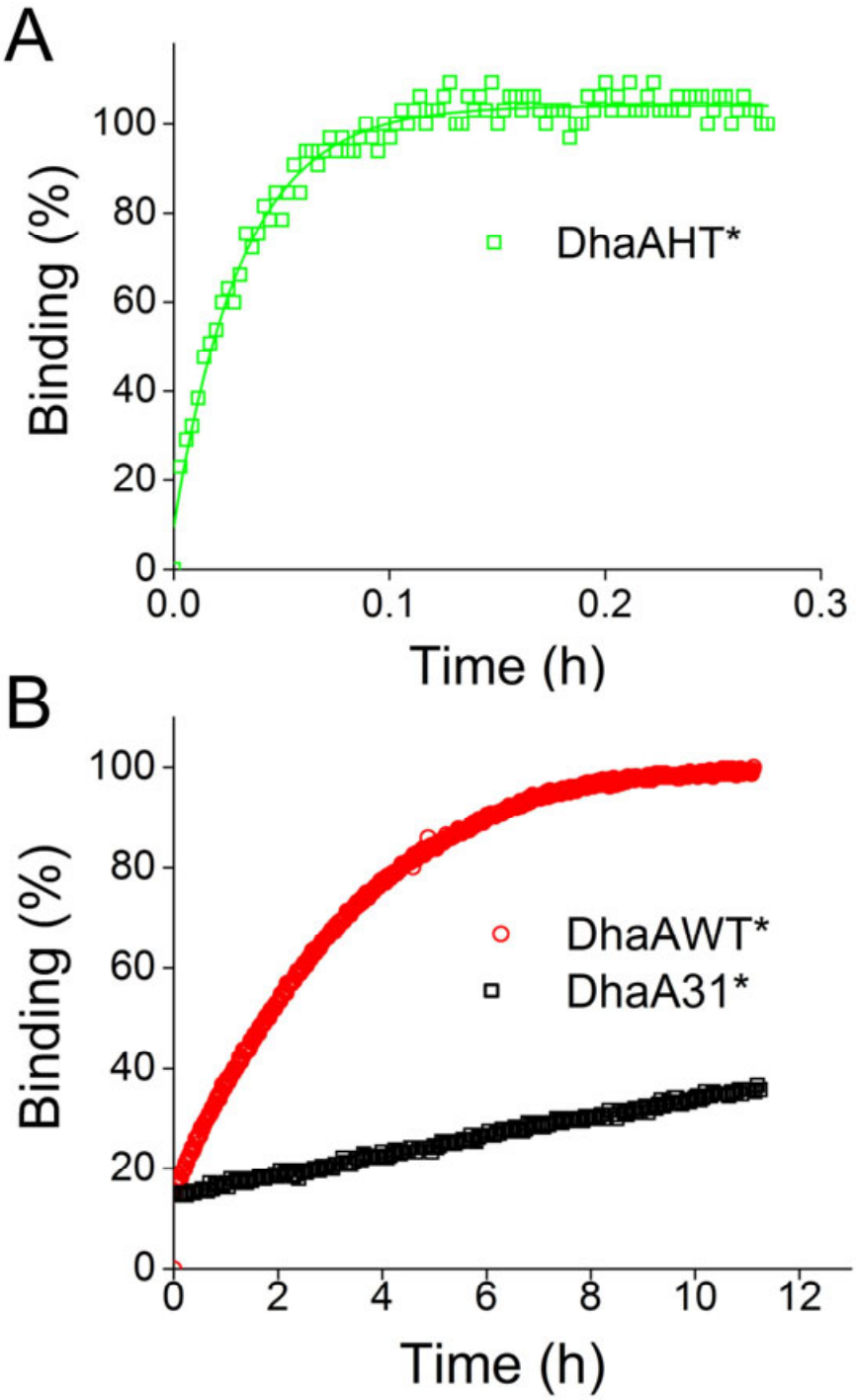

Figure 7. Binding kinetics of TMR ligand in cell free extracts of selected DhaA variants with modified tunnels.

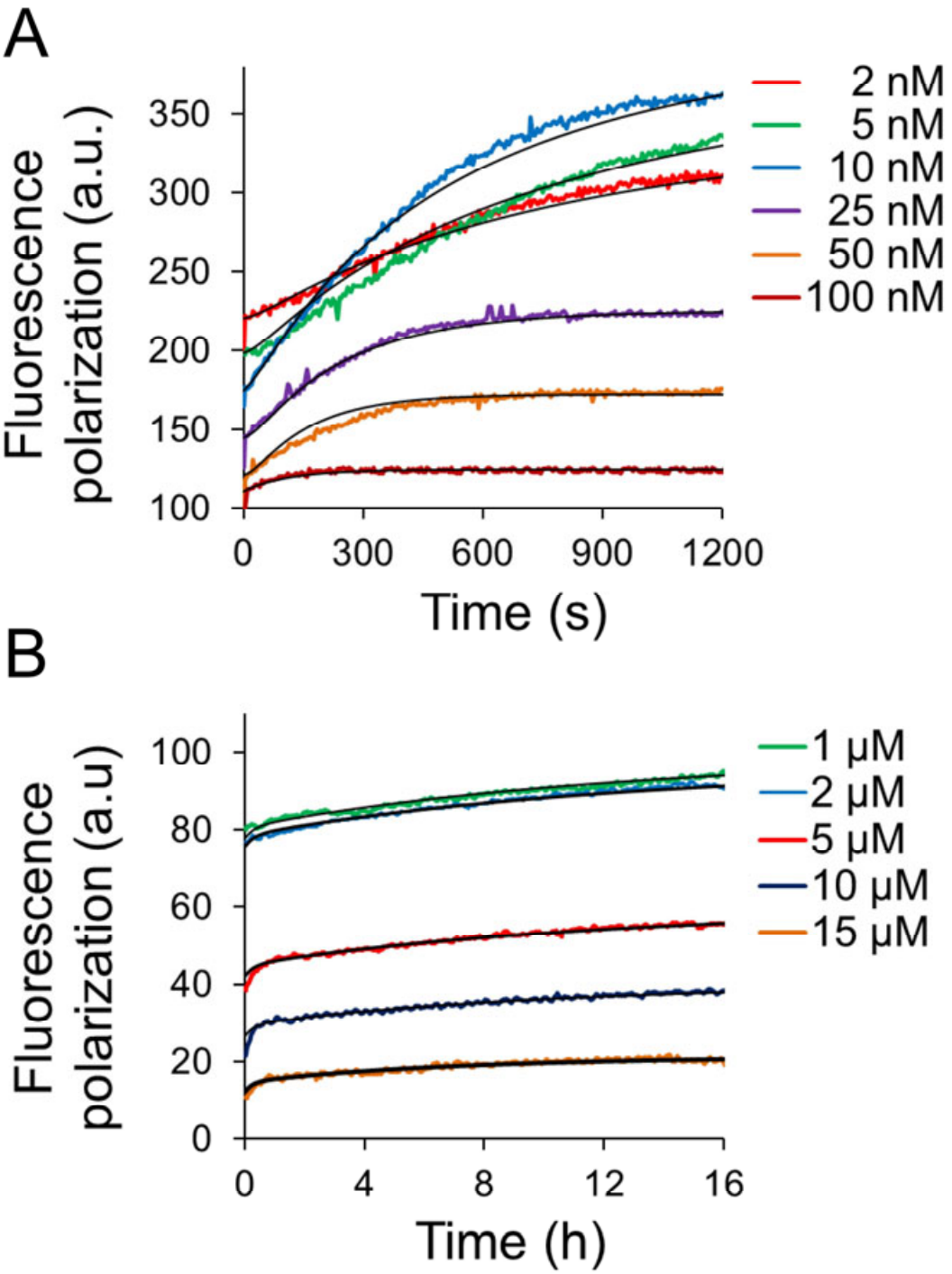

Figure 8. Binding kinetics of TMR ligand to DhaAHT* and DhaA130*. Fluorescence polarization traces obtained upon mixing of DhaAHT* (6 nM) with TMR to final concentration of 2-100 nM (A) and upon mixing of DhaA130* (5 µM) with TMR to final concentration of 1-15 µM (B). Solid lines represent a global fit of Scheme 1 to the kinetic data.